



Article

Robust Leader–Follower Formation Control Using Neural Adaptive Prescribed Performance Strategies

Fengxi Xie ^{1,†} , Guozhen Liang ^{1,†} and Ying-Ren Chien ^{2,*} 

¹ Department of Electrical Engineering and Computer Science, Technische Universität Berlin, 10623 Berlin, Germany; fengxi.xie@campus.tu-berlin.de (F.X.); guozhen.liang@campus.tu-berlin.de (G.L.)

² Department of Electrical Engineering, National Ilan University, Yilan 260007, Taiwan

* Correspondence: yrchien@niu.edu.tw

† These authors contributed equally to this work.

Abstract: This paper introduces a novel leader–follower formation control strategy for autonomous vehicles, aimed at achieving precise trajectory tracking in uncertain environments. The approach is based on a graph guidance law that calculates the desired yaw angles and velocities for follower vehicles using the leader’s reference trajectory, improving system stability and predictability. A key innovation is the development of a Neural Adaptive Prescribed Performance Controller (NA-PPC), which incorporates a Radial Basis Function Neural Network (RBFNN) to approximate nonlinear system dynamics and enhances disturbance estimation accuracy. The proposed method enables high-precision trajectory tracking and formation maintenance under random disturbances, which are vital for autonomous vehicle logistics and detection technologies. Leveraging a graph-based guidance law reduces control complexity and improves robustness against external disturbances. The inclusion of second-order filters and adaptive RBFNNs further enhances nonlinear error handling, improving control performance, stability, and accuracy. The integration of guidance laws, leader–follower control strategies, backstepping techniques, and RBFNNs creates a robust formation control system capable of maintaining performance under dynamic conditions. Comprehensive computer simulations validate the effectiveness of this controller, highlighting its potential to advance autonomous vehicle formation control.



Citation: Xie, F.; Liang, G.; Chien, Y.-R. Robust Leader–Follower Formation Control Using Neural Adaptive Prescribed Performance Strategies. *Mathematics* **2024**, *12*, 3259. <https://doi.org/10.3390/math12203259>

Keywords: autonomous vehicle; trajectory tracking; leader–follower formation control; prescribed performance

MSC: 92C15; 93C40; 93C85

Academic Editors: Marian Barbu, Ramón Vilanova Arbós and Montserrat Gil-Martinez

Received: 29 August 2024
Revised: 9 October 2024
Accepted: 14 October 2024
Published: 17 October 2024



Copyright: © 2024 by the authors. Licensee MDPI, Basel, Switzerland. This article is an open access article distributed under the terms and conditions of the Creative Commons Attribution (CC BY) license (<https://creativecommons.org/licenses/by/4.0/>).

1. Introduction

The coordination of multi-autonomous vehicles has become a significant area of research, with a focus on diverse formation control strategies, including behavior-based control [1], virtual structure [2], and decentralized control [3]. Behavior-based formation control emphasizes local interactions among vehicles to form desired patterns, while virtual structure formation control guides the vehicles to maintain their relative positions within an invisible geometric framework. In decentralized control systems, individual vehicles autonomously make decisions based on locally available information and interactions with neighboring entities. This paper investigates leader–follower formation control for multi-autonomous vehicles, selecting this approach due to its simplicity, ease of implementation, and potential for achieving robust performance under specific conditions [4–6].

A significant amount of research has been conducted on the subject, and a considerable portion of it is of high quality. Yang and Gu [7] implemented nonlinear formation alignment and docking control for a fleet of autonomous underwater vehicles by combining Lyapunov’s direct method with a smooth feedback control law. A leader–follower framework has been employed to develop a guided formation control scheme using a

modular design approach, incorporating concepts from integrator backstepping and cascade theory [8]. These methods are straightforward and relatively easy to implement; however, they encounter significant challenges when subjected to large disturbances. Essentially, these methods lack the capability to autonomously adjust or effectively resist such disturbances, underscoring a significant limitation in their adaptability and robustness. Numerous approaches have been proposed for designing stable controllers, with the sliding mode control (SMC) method emerging as a particularly favored option. SMC is a robust control strategy that effectively mitigates the effects of external disturbances and modeling uncertainties, making it particularly suitable for applications characterized by nonlinear and unpredictable dynamics [9–12]. Wu et al. [10] combined SMC and backstepping techniques to design a closed-loop control system to deal with uncertainty in formation control. Wang et al. [11] introduced a method to address uncertainties by integrating SMC, multi-layer neural networks, and adaptive robust techniques to develop an effective formation controller for underwater vehicles. Also, Su et al. [13] developed an adaptive fixed-time integral sliding mode observer to precisely estimate compound disturbances. However, the implementation of SMC is associated with a significant drawback known as chattering [14].

To address this issue and enhance system robustness, various methods have been proposed, among which the backstepping method is notable. Backstepping control provides a systematic and recursive approach to designing control laws for complex nonlinear systems, ensuring stability while offering flexibility in managing uncertainties and disturbances, thus presenting advantages over SMC [15–17]. The Lyapunov-based backstepping approach has been developed and proven to be able to work effectively [15,16]. Also, Wang et al. [18] built a graph-theory-based backstepping controller to deal with the disturbance. Zaidi et al. [19] combined the chatter-free SMC and backstepping techniques in their design. Yang et al. [20] presented a controller that combines backstepping and SMC techniques to effectively address external disturbances. These combination strategies enhance resistance to perturbations. However, the method imposes a higher computational burden and remains susceptible to instability caused by uncertainty disturbances.

Previous studies have employed Particle Swarm Optimization (PSO), Genetic Algorithm (GA), and Fuzzy Logic Control (FLC) to optimize and effectively address the problem, demonstrating the efficiency of these methods [21–23]. Also, neural network technology is continuously developing and has gained popularity in recent years for handling uncertainty disturbances [24–26]. Neural networks possess the property of universal function approximation, enabling them to approximate any continuously differentiable function. Utilizing Radial Basis Function Neural Networks (RBFNNs) to address uncertainties has been shown to be highly efficient [27,28]. Zhao et al. [29] proposed using RBFNNs and combining Lyapunov–Krasovskii functionals (LKFs) and backstepping techniques as the control scheme. However, if the output of the RBFNN is not fed back to the control system promptly to adjust the control strategy, the stability of the system will be significantly compromised.

To enhance the robustness and adaptive performance of the system by adjusting control inputs based on the error estimates from the RBFNN and clarifying the control decision-making framework, the guidance law emerges as an effective solution [30–32]. Achieving stable performance of the system is challenging; however, a breakthrough was first achieved with the development of the prescribed performance control (PPC) method, despite the inherent difficulties in maintaining stable system performance. The core concept of attaining predetermined levels of transient and steady-state performance in tracking output errors is captured by an innovative PPC approach introduced in [33], employing a transformation function that strictly increases or decreases the tracking error. Recently, more PPC methods have been developed [20,34–36]. They have achieved good results, but the challenge for formation control remains [37]. Mehdifar et al. [38] introduced a distributed graph-based formation control method for leader–follower multi-agent systems, employing a prescribed performance strategy that achieved promising results. Nevertheless, the method does not account for external disturbances. Dai et al. [37] incorporates

barrier Lyapunov functions and an adaptive backstepping procedure to ensure the stability of the closed-loop systems while maintaining performance within specified bounds. The barrier Lyapunov Function is essential when state constraints must be strictly enforced, while a conventional Lyapunov function is sufficient for general stability without explicit state constraints. However, their method heavily relies on the accuracy of dynamic modeling, which implies that its robustness and adaptability may be limited. Jiang et al. [36] suggested a prescribed-time formation control approach for second-order nonlinear multi-agent systems with a directed graph. Nonetheless, potential remains for further optimization of the system responsiveness. In summary, the formation members have limited communication capabilities, and complex algorithms may impede controller performance. Moreover, accurately approximating disturbances poses a challenge, which can affect the robustness and adaptability of a system [6,39,40].

In this paper, a controller is proposed for autonomous vehicle formation control, combining the leader–follower method and backstepping technique. The predefined trajectory of the leader and the desired formation shape direct the generation of desired yaw angles and velocities for the followers through a graph-based guidance law. Nonlinear error handling is achieved through a second-order filter and RBFNN, complemented by an adaptive law. Furthermore, a barrier Lyapunov function is utilized to accomplish controlled performance objectives.

Despite significant progress in vehicle formation control, many existing methods struggle to maintain precise trajectory tracking and formation under random disturbances or unknown nonlinearities. Additionally, these approaches often do not adequately address the balance between control complexity and system robustness in highly dynamic environments. Previous studies have also lacked detailed comparisons with methods using predefined performance constraints (PPCs), which are crucial for evaluating real-world effectiveness.

The key contributions of this work are summarized as follows: (1) This work enables precise trajectory tracking and formation maintenance under random disturbances, addressing a key limitation in current autonomous vehicle formation control methods. This contribution is particularly relevant to future logistics and autonomous vehicle detection technologies. (2) A graph-based guidance law is designed for preemptive input optimization and adjustment, reducing control complexity and significantly enhancing system robustness, allowing PPC systems to handle external variations more effectively and maintain predetermined performance standards. (3) The use of second-order filters and RBFNNs effectively handles nonlinear errors, improving control performance by mitigating nonlinearities, enhancing stability, and tracking accuracy. The adaptive law further enhances adaptability to changing dynamics. (4) This approach successfully integrates the guidance law, leader–follower control, backstepping technique, and RBFNNs to achieve robust formation control under external random disturbances, increasing system robustness while decreasing controller complexity.

The remainder of this study is organized as follows: In Section 2, the kinetic and dynamic model of the vehicle is presented. Section 3 outlines the development of the proposed controller, utilizing a Lyapunov function to establish stability. Section 4 details the simulation outcomes for formation trajectory tracking under external disturbances. Finally, Section 5 provides a summary and the conclusions of this study.

2. Kinematics and Dynamics Models

Referring to Figure 1, the kinematics and dynamics of the i -th vehicle can be expressed as follows:

$$\begin{cases} \dot{x}_i = v_i \cos(\theta_i) \\ \dot{y}_i = v_i \sin(\theta_i) \\ \dot{\theta}_i = \sigma_i^{-1} v_i \tan(\delta_i) + f_{\theta,i}(\theta_i) + d_{\theta,i} \\ \dot{v}_i = F_i + f_{v,i}(v_i) + d_{v,i} \end{cases} \quad (1)$$

where the constant $\sigma_i > 0$ is the length of the i -th vehicle; (x_i, y_i) denotes the reference point of the i -th vehicle positioned at the midpoint of the rear axle; $x_i \in \mathbb{R}$ represents the longitudinal position; and $y_i \in (-a, a)$ denotes the lateral position of the vehicle in an inertial frame with Cartesian coordinates (X, Y) . The speed of the i -th vehicle at point (x_i, y_i) is denoted by v_i , while $\theta_i \in (-\frac{\pi}{2}, \frac{\pi}{2})$ represents the angular orientation of the vehicle relative to the X axis. The steering angle of the front wheels relative to the orientation of the i -th vehicle θ_i is denoted by δ_i , and the acceleration of the i -th vehicle is denoted by F_i . Note that $f_{\theta,i}(\theta_i)$ and $f_{v,i}(v_i)$ are unknown nonlinear functions; $d_{\theta,i}(t)$ and $d_{v,i}(t)$ denote the unknown and bounded external disturbances, respectively.

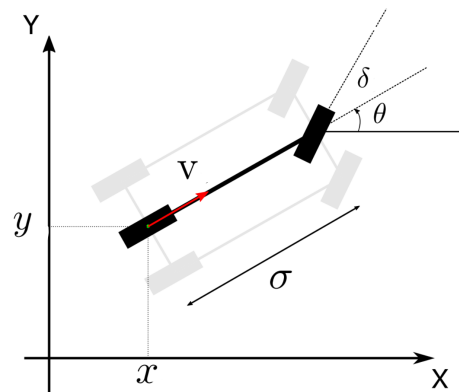


Figure 1. Vehicle model.

Lemma 1. The nonlinear function $g(x)$ can be approximated by an RBFNN with a specified accuracy $\bar{\epsilon} > 0$. Specifically, $g(x)$ is expressed as

$$g(x) = W^T \varphi(x) + \epsilon(x),$$

where $W \in R^{l \times 1}$ represents the ideal constant weight matrix, and $\epsilon(x) \in R^1$ is the approximation error satisfying $|\epsilon(x)| \leq \bar{\epsilon}$. Here, $\varphi(x) = (\varphi_1(x), \varphi_2(x), \dots, \varphi_l(x))^T$ denotes the vector of Gaussian basis function, where $\varphi_j(x) = \exp\left(-\frac{\|x - c_j\|^2}{2\sigma_j^2}\right)$, for $j = 1, 2, \dots, l$, with c_j and σ_j representing the center and width of the Gaussian basis function $\varphi_j(x)$, respectively. Here, $x = (x_1, x_2, \dots, x_q)^T$. Furthermore, there is $\|\varphi(x)\|^2 \leq \|\varphi(\dot{x})\|^2$, where $\dot{x} = (\dot{x}_1, \dot{x}_2, \dots, \dot{x}_r)^T, r \leq q$.

Lemma 2. For all $a, b \geq 0$, and $p, q > 0$, with $1/p + 1/q = 1$, the inequality $ab \leq \frac{a^p}{p} + \frac{b^q}{q}$ is satisfied.

3. Controller Design

In this section, a formation tracking controller is proposed for the vehicle formation members. Figure 2 describes the structure and the workflow of the proposed system. Figure 3 illustrates the geometric relationship between the leader and the i -th follower and shows how the leader–follower mechanism works, where the i -th member follows the leader as its follower. The whole system is designed using the backstepping technique. Given the desired trajectory of the leader and considering the kinematics and dynamics involved, the desired velocity and steering angle are formulated and subsequently integrated into the guidance law. Subsequently, the desired yaw angle $\theta_{d,i}$ and velocity $v_{d,i}$ for the followers are calculated, which are then used as inputs to their respective steering angle and velocity controllers. To ensure high robustness against unknown disturbances, a second-order filter is employed to estimate the error, and an RBFNN is used to approximate the unknown nonlinear function. For this purpose, an adaptive law is designed. Additionally, a nominal function is considered in the system, and another adaptive law is introduced to handle it. Finally, the final desired steering angle and velocity are computed to guide the followers effectively.

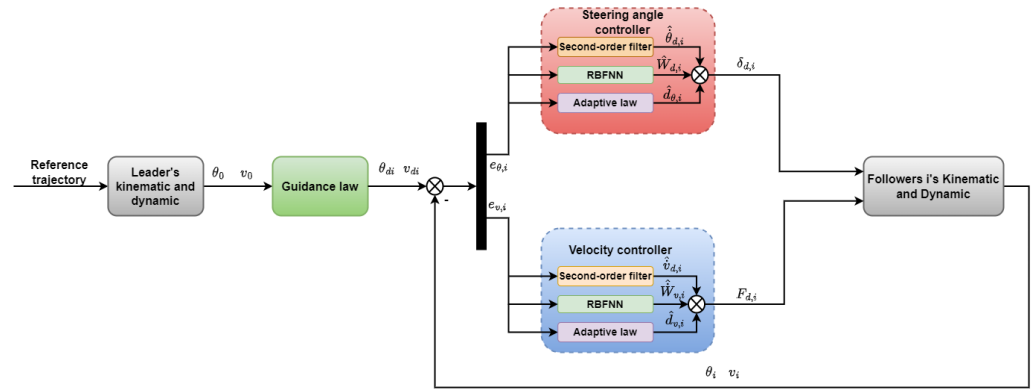


Figure 2. Proposed formation controller design.

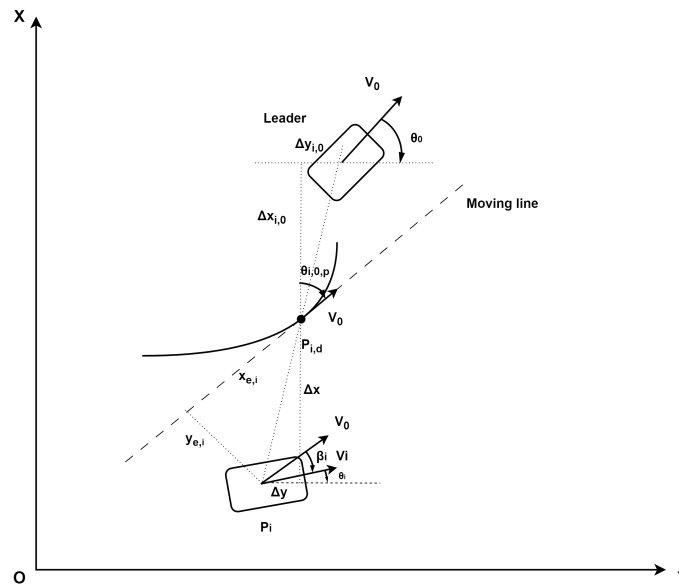


Figure 3. Formation control of the geometric relationship between leader and *i*-th follower.

3.1. Guidance Law Design

The guidance law is specifically formulated to enhance the flexibility and adaptability of the system. In this paper, the desired shape of the formation is predefined, while the initial positions of the formation members are randomized. For illustration, consider the scenario involving a leader and one of its followers (denoted as *i*). The current position of follower *i* is represented as p_i , while $p_{i,d}$ signifies its desired position. The desired position vector $p_{i,d} = [x_{i,d}, y_{i,d}]^T = [x_i, y_i]^T + [\Delta x, \Delta y]^T$.

Referring to Figure 3, the objective is to effectively control the *i*-th member, ensuring that p_i converges to the target position. To achieve this, an error term is defined with the objective of driving it to convergence as follows:

$$\begin{bmatrix} x_{e,i} \\ y_{e,i} \end{bmatrix} = \begin{bmatrix} \cos \theta_{i,0,p} & -\sin \theta_{i,0,p} \\ \sin \theta_{i,0,p} & \cos \theta_{i,0,p} \end{bmatrix}^T (p_i - p_{i,d}), \tag{2}$$

where $\theta_{i,0,p} = \text{atan2}(y'_i + \Delta y', x'_i + \Delta x') \in [-\pi, \pi]$, $y_{e,i}$ denotes the minimum distance between the current position p_i of vehicle *i* and the trajectory path of its desired position $p_{i,d}$, and $x_{e,i}$ denotes the distance along the trajectory line between the actual position p_i of the vehicle *i* and the moving line of the desired position $p_{i,d}$.

Minimizing the error requires precise calculation. The derivative of $y_{e,i}$ is obtained as follows:

$$\dot{y}_{e,i} = v_i \sin(\theta_i - \theta_{p,i}). \tag{3}$$

The barrier Lyapunov function is used in the design of the control law to constrain the error and ensure the controlled member remains stable during motion. Additionally, distinct Lyapunov candidates are designed for $y_{e,i}$ and $x_{e,i}$ to minimize interference between the different error terms. A Lyapunov function for $y_{e,i}$ is presented as follows:

$$V_1 = \frac{b_{y,i}^2}{\pi} \tan\left(\frac{\pi y_{e,i}^2}{2b_{y,i}^2}\right), \tag{4}$$

where $b_{y,i}$ is the upper boundary of $y_{e,i}$.

By taking the derivative of Equation (4), one can prove the stability of V_1 as follows:

$$\dot{V}_1 = \frac{y_{e,i}\dot{y}_{e,i}}{\cos^2\left(\frac{\pi y_{e,i}^2}{2b_{y,i}^2}\right)} + \frac{2b_{y,i}\dot{b}_{y,i}}{\pi} \tan\left(\frac{\pi y_{e,i}^2}{2b_{y,i}^2}\right) - \left(\frac{\dot{b}_{y,i}}{b_{y,i}}\right) \frac{y_{e,i}^2}{\cos^2\left(\frac{\pi y_{e,i}^2}{2b_{y,i}^2}\right)}. \tag{5}$$

Using the vector field guidance principle, the desired yaw angle can be formulated $\theta_{d,i}$ as follows:

$$\theta_{d,i} = \theta_{p,i} + \arcsin\left(-\frac{k_y b_{y,i}^2}{2v_i \pi y_{e,i}} \sin\left(\frac{\pi y_{e,i}^2}{b_{y,i}^2}\right) + \frac{\dot{b}_{y,i}}{v_i b_{y,i}} y_{e,i}\right), \tag{6}$$

where $k_y > 0$ is the guidance law parameter, representing the strength of the vector field.

According to Equations (3) and (6), Equation (5) can be rewritten as Equation (7).

$$\begin{aligned} \dot{V}_1 &= \frac{y_{e,i}\dot{y}_{e,i}}{\cos^2\left(\frac{\pi y_{e,i}^2}{2b_{y,i}^2}\right)} + \frac{2b_{y,i}\dot{b}_{y,i}}{\pi} \tan\left(\frac{\pi y_{e,i}^2}{2b_{y,i}^2}\right) - \left(\frac{\dot{b}_{y,i}}{b_{y,i}}\right) \frac{y_{e,i}^2}{\cos^2\left(\frac{\pi y_{e,i}^2}{2b_{y,i}^2}\right)} \\ &\leq \frac{y_{e,i}\dot{y}_{e,i}}{\cos^2\left(\frac{\pi y_{e,i}^2}{2b_{y,i}^2}\right)} - \left(\frac{\dot{b}_{y,i}}{b_{y,i}}\right) \frac{y_{e,i}^2}{\cos^2\left(\frac{\pi y_{e,i}^2}{2b_{y,i}^2}\right)} + \frac{2k_b b_{y,i}^2}{\pi} \tan\left(\frac{\pi y_{e,i}^2}{2b_{y,i}^2}\right) \\ &\leq \frac{y_{e,i}v_i \sin(\theta_i - \theta_{p,i})}{\cos^2\left(\frac{\pi y_{e,i}^2}{2b_{y,i}^2}\right)} - \left(\frac{\dot{b}_{y,i}}{b_{y,i}}\right) \frac{y_{e,i}^2}{\cos^2\left(\frac{\pi y_{e,i}^2}{2b_{y,i}^2}\right)} + \frac{2k_b b_{y,i}^2}{\pi} \tan\left(\frac{\pi y_{e,i}^2}{2b_{y,i}^2}\right) \\ &\leq \frac{y_{e,i} \left(-\frac{k_d b_{y,i}^2}{2\pi y_{e,i}} \sin\left(\frac{\pi y_{e,i}^2}{b_{y,i}^2}\right) + \frac{\dot{b}_{y,i}}{b_{y,i}} y_{e,i}\right)}{\cos^2\left(\frac{\pi y_{e,i}^2}{2b_{y,i}^2}\right)} - \left(\frac{\dot{b}_{y,i}}{b_{y,i}}\right) \frac{y_{e,i}^2}{\cos^2\left(\frac{\pi y_{e,i}^2}{2b_{y,i}^2}\right)} + \frac{2k_b b_{y,i}^2}{\pi} \tan\left(\frac{\pi y_{e,i}^2}{2b_{y,i}^2}\right) \\ &\leq -(k_d - 2k_b) \frac{b_{y,i}^2}{\pi} \tan\left(\frac{\pi y_{e,i}^2}{2b_{y,i}^2}\right), \end{aligned} \tag{7}$$

where $k_b = \sup\left|\frac{\dot{b}_{y,i}}{b_{y,i}}\right|$.

By choosing $k_d > 2k_b$, the following inequality holds:

$$\dot{V}_1 \leq -c_1 V_1, \tag{8}$$

where $c_1 = k_d - 2k_b$.

From Figure 3, the derivative of $x_{e,i}$ can be obtained as follows:

$$\dot{x}_{e,i} = v_0 - v_i \cos \beta_i. \tag{9}$$

A Lyapunov function for $x_{e,i}$ is presented as follows:

$$V_2 = \frac{b_{x,i}^2}{\pi} \tan\left(\frac{\pi x_{e,i}^2}{2b_{x,i}^2}\right), \tag{10}$$

where $b_{x,i}$ is the upper boundary of $x_{e,i}$. Additionally, in accordance with the guidance law, the desired velocity is formulated as follows:

$$v_{d,i} = \frac{1}{\cos \beta_i} \left(\frac{k_v b_{x,i}^2}{2\pi x_{e,i}} \sin\left(\frac{\pi x_{e,i}^2}{b_{x,i}^2}\right) - \frac{\dot{b}_{x,i}}{b_{x,i}} x_{e,i} + v_j \right), \tag{11}$$

where $\beta_i = \theta_i - \theta_{pi}$.

Upon differentiating Equation (10), the resulting expression for \dot{V}_2 is given by Equation (12).

$$\begin{aligned} \dot{V}_2 &= \frac{x_{e,i} \dot{x}_{e,i}}{\cos^2\left(\frac{\pi x_{e,i}^2}{2b_{x,i}^2}\right)} + \frac{2b_{x,i} \dot{b}_{x,i}}{\pi} \tan\left(\frac{\pi x_{e,i}^2}{2b_{x,i}^2}\right) - \left(\frac{\dot{b}_{x,i}}{b_{x,i}}\right) \frac{x_{e,i}^2}{\cos^2\left(\frac{\pi x_{e,i}^2}{2b_{x,i}^2}\right)} \\ &\leq \frac{x_{e,i} \dot{x}_{e,i}}{\cos^2\left(\frac{\pi x_{e,i}^2}{2b_{x,i}^2}\right)} - \left(\frac{\dot{b}_{x,i}}{b_{x,i}}\right) \frac{x_{e,i}^2}{\cos^2\left(\frac{\pi x_{e,i}^2}{2b_{x,i}^2}\right)} + \frac{2k_c b_{x,i}^2}{\pi} \tan\left(\frac{\pi x_{e,i}^2}{2b_{x,i}^2}\right) \\ &\leq \frac{x_{e,i} (v_j - v_i \cos \beta_i)}{\cos^2\left(\frac{\pi x_{e,i}^2}{2b_{x,i}^2}\right)} - \left(\frac{\dot{b}_{x,i}}{b_{x,i}}\right) \frac{x_{e,i}^2}{\cos^2\left(\frac{\pi x_{e,i}^2}{2b_{x,i}^2}\right)} + \frac{2k_c b_{x,i}^2}{\pi} \tan\left(\frac{\pi x_{e,i}^2}{2b_{x,i}^2}\right) \\ &\leq -(k_v - 2k_c) \frac{b_{x,i}^2}{\pi} \tan\left(\frac{\pi x_{e,i}^2}{2b_{x,i}^2}\right), \end{aligned} \tag{12}$$

where $k_c = \sup \left| \frac{\dot{b}_{x,i}}{b_{x,i}} \right|$.

By selecting $k_v > 2k_c$, the following can be additionally derived:

$$\dot{V}_2 \leq -c_2 V_2, \tag{13}$$

where $c_2 = k_v - 2k_c$.

3.2. Steering Angle Controller Design

With the guidance law providing the desired yaw angle and velocity, it is essential to design controllers for these parameters. These controllers are developed independently, offering several practical advantages, including modularity, specialization, simplicity, robustness, and scalability. For the i -th formation member, the angle error is defined as follows:

$$e_{\theta,i} = \theta_i - \theta_{d,i}. \tag{14}$$

Note that the computations of the derivatives of $\theta_{d,i}$ are extremely intricate. Therefore, a second-order filter is introduced to mitigate this complexity as follows:

$$\begin{cases} \dot{\Phi}_{10} = \Phi_{20} \\ \dot{\Phi}_{20} = -2\zeta_0 \omega_{n0} \Phi_{20} - \omega_n^2 (\Phi_{10} - \theta_{d,i})' \end{cases} \tag{15}$$

where the damping rate ζ_0 and frequency ω_{n0} are predetermined constants, $\theta_{d,i}$ represents the input, Φ_{10} is the output and an estimation of $\theta_{d,i}$, and Φ_{20} can be interpreted as the derivative of $\theta_{d,i}$, denoted as $\hat{\theta}_{d,i}$. The estimated error of this second-order filter is defined as follows:

$$\tilde{\theta}_{d,i} = \hat{\theta}_{d,i} - \theta_{d,i}. \tag{16}$$

Consider a Lyapunov candidate

$$V_0 = \frac{1}{2}e_{\theta,i}^2 \tag{17}$$

and refer to Equations (1) and (16). The derivative of V_0 can be expressed as follows:

$$\begin{aligned} \dot{V}_0 &= e_{\theta,i}\dot{e}_{\theta,i} \\ &= e_{\theta,i}(\dot{\theta}_i - \dot{\theta}_{d,i}) \\ &= e_{\theta,i}\left(\sigma_i^{-1}v_i \tan(\delta_i) + f_{\theta,i} + d_{\theta,i} - \hat{\theta}_{d,i} - \tilde{\theta}_{d,i}\right). \end{aligned} \tag{18}$$

RBFNN is a type of artificial neural network that is commonly used for function approximation and pattern recognition tasks. The network architecture consists of three layers: an input layer, a hidden layer utilizing radial basis functions, and an output layer. In this control system, the RBFNN helps to handle unknown nonlinearities by compensating for steering angle errors. The steering angle error $e_{\theta,i}$ is fed into the RBFNN, which processes it using radial basis functions. The RBFNN generates a compensation signal by combining the responses from different nodes. The network adjusts its weights in real time using an adaptive law, allowing it to better approximate the nonlinearities in the system as conditions change. Finally, the RBFNN output, along with other control factors, is used to update the steering angle. This ensures the vehicle stays on its desired path, even when facing disturbances or changing conditions. The adaptive nature of the RBFNN makes the system more robust and responsive. Consequently, this process can be expressed as follows:

$$\begin{aligned} \dot{V}_0 &= e_{\theta,i}\left(\sigma_i^{-1}v_i \tan(\delta_i) + W_{\theta,i}\varphi_{\theta,i} + \varepsilon_{\theta,i} + d_{\theta,i} - \hat{\theta}_{d,i} - \tilde{\theta}_{d,i}\right) \\ &= e_{\theta,i}\left(\sigma_i^{-1}v_i \tan(\delta_i) + W_{\theta,i}\varphi_{\theta,i} - \hat{\theta}_{d,i} + \tilde{d}_{\theta,i}\right), \end{aligned} \tag{19}$$

where $\tilde{d}_{\theta,i} = \varepsilon_{\theta,i} + d_{\theta,i} - \tilde{\theta}_{d,i}$ represents total disturbances. It is evident that $\tilde{d}_{\theta,i}$ is bounded, adhering to $\tilde{d}_{\theta,i} \leq \bar{d}_{\theta,i}$. Furthermore, $\hat{W}_{\theta,i} = W_{\theta,i} - \tilde{W}_{\theta,i}$ and $W_{\theta,i} \leq \bar{W}_{\theta,i}$.

To deal with the unknown nonlinear functions, the adaptive law is designed as follows:

$$\dot{\hat{W}}_{\theta,i} = k_{1,\theta,i}(\varphi_{\theta,i}e_{\theta,i} - k_{2,\theta,i}\hat{W}_{\theta,i}) \tag{20}$$

with positive parameters $k_{1,\theta,i}$ and $k_{2,\theta,i}$.

To deal with nominal disturbance, another adaptive law is designed as follows:

$$\dot{\hat{d}}_{\theta,i} = k_{3,\theta,i}(e_{\theta,i} - k_{4,\theta,i}\hat{d}_{\theta,i}) \tag{21}$$

with positive parameters $k_{3,\theta,i}$ and $k_{4,\theta,i}$.

For the adaptive tracking controller, the intended steering angle of the front wheels can be formulated as follows:

$$\delta_{d,i} = \arctan\left(v_i^{-1}\sigma_i(-k_{5,\theta,i}e_{\theta,i} - \hat{d}_{\theta,i} - \hat{W}_{\theta,i}\varphi_{\theta,i} + \hat{\theta}_{d,i})\right). \tag{22}$$

Consider a Lyapunov candidate given by the following:

$$V_3 = \frac{1}{2}e_{\theta,i}^2 + \frac{1}{2}k_{3,\theta,i}^{-1}\tilde{d}_{\theta,i}^2 + \frac{1}{2}k_{1,\theta,i}^{-1}\tilde{W}_{\theta,i}^2, \tag{23}$$

where $\tilde{d} = \bar{d} - \hat{d}$. After some straightforward manipulation, the time derivative of V_3 can be expressed as Equation (24) as follows:

$$\begin{aligned}
 \dot{V}_3 &= e_{\theta,i} \dot{e}_{\theta,i} + \hat{d}_{\theta,i} \dot{\hat{d}}_{\theta,i} + \tilde{W}_{\theta,i} \dot{\tilde{W}}_{\theta,i} \\
 &= e_{\theta,i} \left(\sigma_i^{-1} v_i \tan(\delta_i) + W_{\theta,i} \varphi_{\theta,i} - \hat{\theta}_{d,i} + \tilde{d}_{\theta,i} \right) + \hat{d}_{\theta,i} \left(e_{\theta,i} - k_{4,\theta,i} \hat{d}_{\theta,i} \right) - \tilde{W}_{\theta,i} \dot{\tilde{W}}_{\theta,i} \\
 &= e_{\theta,i} \left(-k_{5,\theta,i} e_{\theta,i} - \hat{d}_{\theta,i} - \hat{W}_{\theta,i} \varphi_{\theta,i} + W_{\theta,i} \varphi_{\theta,i} + \tilde{d}_{\theta,i} \right) + \hat{d}_{\theta,i} \left(e_{\theta,i} - k_{4,\theta,i} \hat{d}_{\theta,i} \right) \\
 &\quad - \tilde{W}_{\theta,i} \left(\varphi_{\theta,i} e_{\theta,i} - k_{2,\theta,i} \tilde{W}_{\theta,i} \right) \\
 &\leq -k_{5,\theta,i} e_{\theta,i}^2 - k_{4,\theta,i} \hat{d}_{\theta,i}^2 + e_{\theta,i} \tilde{d}_{\theta,i} + k_{2,\theta,i} \tilde{W}_{\theta,i} \hat{W}_{\theta,i} \\
 &\leq -k_{5,\theta,i} e_{\theta,i}^2 - k_{4,\theta,i} \hat{d}_{\theta,i}^2 + e_{\theta,i} \tilde{d}_{\theta,i} + k_{2,\theta,i} \|\tilde{W}_{\theta,i}\| \|\hat{W}_{\theta,i}\| \\
 &\leq -k_{5,\theta,i} e_{\theta,i}^2 - k_{4,\theta,i} \hat{d}_{\theta,i}^2 + e_{\theta,i} \tilde{d}_{\theta,i} + k_{2,\theta,i} \|\tilde{W}_{\theta,i}\| (\bar{W}_{\theta,i} - \|\tilde{W}_{\theta,i}\|),
 \end{aligned} \tag{24}$$

where $\|W_{\theta,i}\| \leq \bar{W}_{\theta,i}$.

Utilizing Lemma 2, the following inequalities can be described as follows:

$$\|\tilde{W}_{\theta,i}\| (\bar{W}_{\theta,i} - \|\tilde{W}_{\theta,i}\|) \leq -\frac{1}{2} \|\tilde{W}_{\theta,i}\|^2 + \frac{1}{2} \bar{W}_{\theta,i}^2 \tag{25}$$

and

$$e_{\theta,i} \tilde{d}_{\theta,i} \leq \frac{1}{2} \|e_{\theta,i}\|^2 + \frac{1}{2} \tilde{d}_{\theta,i}^2. \tag{26}$$

Then, by combining the inequalities Equations (25) and (26), Equation (24) can be reformulated as follows:

$$\begin{aligned}
 \dot{V}_3 &\leq -k_{5,\theta,i} e_{\theta,i}^2 - k_{4,\theta,i} \hat{d}_{\theta,i}^2 - \frac{1}{2} k_{2,\theta,i} \|\tilde{W}_{\theta,i}\|^2 + \frac{1}{2} \|e_{\theta,i}\|^2 + \frac{1}{2} \tilde{d}_{\theta,i}^2 + k_{2,\theta,i} \frac{1}{2} \|\tilde{W}_{\theta,i}\|^2 \\
 &\leq -\left(k_{5,\theta,i} - \frac{1}{2}\right) e_{\theta,i}^2 - k_{4,\theta,i} \hat{d}_{\theta,i}^2 - \frac{1}{2} k_{2,\theta,i} \|\tilde{W}_{\theta,i}\|^2 + \frac{1}{2} \tilde{d}_{\theta,i}^2 + k_{2,\theta,i} \frac{1}{2} \|\tilde{W}_{\theta,i}\|^2.
 \end{aligned} \tag{27}$$

From Equation (27), it can be concluded that $\dot{V}_3 \leq -\sigma_3 V_3 + \zeta_1$, where $\sigma_3 = \min\{k_{5,\theta,i} - \frac{1}{2}, k_{4,\theta,i}, k_{2,\theta,i}\} > 0$ and $\zeta_1 = \frac{1}{2} \tilde{d}_{\theta,i}^2 + k_{2,\theta,i} \frac{1}{2} \|\tilde{W}_{\theta,i}\|^2 > 0$.

3.3. Velocity Controller Design

For formation members, the velocity error is defined as follows:

$$e_{v,i} = v_i - v_{d,i}. \tag{28}$$

Note that the computations of the derivatives of $v_{d,i}$ are extremely intricate. Therefore, a second-order filter is introduced to mitigate this issue as follows:

$$\begin{cases} \dot{\Phi}_{30} = \Phi_{40} \\ \dot{\Phi}_{40} = -2\zeta_0 \omega_{n0} \Phi_{40} - \omega_n^2 (\Phi_{10} - v_{d,i}), \end{cases} \tag{29}$$

where damp rate ζ_0 and frequency ω_{n0} are designed constants, $v_{d,i}$ is the input, Φ_{30} is the output and the estimation of $v_{d,i}$, and Φ_{40} can be taken as the derivative of $v_{d,i}$ which is denoted as $\hat{v}_{d,i}$. The estimation error for this second-order filter is characterized as follows:

$$\tilde{v}_{d,i} = \hat{v}_{d,i} - v_{d,i}. \tag{30}$$

By taking the derivative of the velocity error,

$$\begin{aligned}
 \dot{e}_{v,i} &= \dot{v}_i - \dot{v}_{d,i} \\
 &= F_i + f_{v,i}(v_i) + d_{v,i} - \hat{v}_{d,i} - \tilde{v}_{d,i}.
 \end{aligned} \tag{31}$$

Again, the unknown nonlinear functions can be approximated by employing an RBFNN as follows:

$$\begin{aligned} \dot{e}_{v,i} &= F_i + W_{v,i}\varphi_{v,i} + \varepsilon_{v,i} + d_{v,i} - \hat{v}_{d,i} - \tilde{v}_{d,i} \\ &= F_i + W_{v,i}\varphi_{v,i} + d_{v,i} - \hat{v}_{d,i} + \tilde{d}_{v,i} \end{aligned} \tag{32}$$

where $\tilde{d}_{v,i} = \varepsilon_{v,i} + d_{v,i} - \tilde{v}_{d,i}$ is the total disturbance. Apparently, $\tilde{d}_{v,i}$ is bounded, satisfying $\tilde{d}_{v,i} \leq \bar{d}_{v,i}$. $\tilde{W}_{v,i} = W_{v,i} - \hat{W}_{v,i}$ and $W_{v,i} \leq \bar{W}_{v,i}$.

To deal with the unknown nonlinear functions, the adaptive law is designed as follows:

$$\dot{\hat{W}}_{v,i} = k_{1,v,i}(\varphi_{v,i}e_{v,i} - k_{2,v,i}\hat{W}_{v,i}) \tag{33}$$

with positive parameters $k_{1,v,i}$ and $k_{2,v,i}$.

To deal with nominal disturbance, another adaptive law is designed as

$$\dot{\hat{d}}_{v,i} = k_{3,v,i}(e_{v,i} - k_{4,v,i}\hat{d}_{v,i}) \tag{34}$$

with positive parameters $k_{3,v,i}$ and $k_{4,v,i}$. The adaptive tracking controller for the desired velocity can be formulated as follows:

$$F_{d,i} = -k_{5,v,i}e_{v,i} - \hat{d}_{v,i} - \hat{W}_{v,i}\varphi_{v,i} + \hat{v}_{d,i}. \tag{35}$$

Consider a Lyapunov candidate

$$V_4 = \frac{1}{2}e_{v,i}^2 + \frac{1}{2}k_{3,v,i}^{-1}\hat{d}_{v,i}^2 + \frac{1}{2}k_{1,v,i}^{-1}\tilde{W}_{v,i}^2. \tag{36}$$

Then, by combining Equations (31), (33) and (34), the differential of V_4 can be described as Equation (37) as follows:

$$\begin{aligned} \dot{V}_4 &= e_{v,i}\dot{e}_{v,i} + \hat{d}_{v,i}\dot{\hat{d}}_{v,i} + \tilde{W}_{v,i}\dot{\tilde{W}}_{v,i} \\ &= e_{v,i}(F_i + W_{v,i}\varphi_{v,i} - \hat{v}_{d,i} + \tilde{d}_{v,i}) + \hat{d}_{v,i}(e_{v,i} - k_{4,v,i}\hat{d}_{v,i}) - \tilde{W}_{v,i}\dot{\tilde{W}}_{v,i} \\ &= e_{v,i}(-k_{5,v,i}e_{v,i} - \hat{d}_{v,i} - \hat{W}_{v,i}\varphi_{v,i} + W_{v,i}\varphi_{v,i} + \tilde{d}_{v,i}) + \hat{d}_{v,i}(e_{v,i} - k_{4,v,i}\hat{d}_{v,i}) \\ &\quad - \tilde{W}_{v,i}(\varphi_{v,i}e_{v,i} - k_{2,v,i}\hat{W}_{v,i}) \\ &\leq -k_{5,v,i}e_{v,i}^2 - k_{4,v,i}\hat{d}_{v,i}^2 + e_{v,i}\bar{d}_{v,i} + k_{2,v,i}\tilde{W}_{v,i}\hat{W}_{v,i} \\ &\leq -k_{5,v,i}e_{v,i}^2 - k_{4,v,i}\hat{d}_{v,i}^2 + e_{v,i}\bar{d}_{v,i} + k_{2,v,i}\|\tilde{W}_{v,i}\|\|\hat{W}_{v,i}\| \\ &\leq -k_{5,v,i}e_{v,i}^2 - k_{4,v,i}\hat{d}_{v,i}^2 + e_{v,i}\bar{d}_{v,i} + k_{2,v,i}\|\tilde{W}_{v,i}\|(\bar{W}_{v,i} - \|\tilde{W}_{v,i}\|), \end{aligned} \tag{37}$$

where $\|\tilde{W}_{v,i}\| \leq \bar{W}_{v,i}$.

Utilizing Lemma 2, the following inequalities can be derived.

$$\|\tilde{W}_{v,i}\|(\bar{W}_{v,i} - \|\tilde{W}_{v,i}\|) \leq -\frac{1}{2}\|\tilde{W}_{v,i}\|^2 + \frac{1}{2}\bar{W}_{v,i}^2 \tag{38}$$

and

$$e_{v,i}\bar{d}_{v,i} \leq \frac{1}{2}\|e_{v,i}\|^2 + \frac{1}{2}\bar{d}_{v,i}^2. \tag{39}$$

Combining inequalities (38) and (39), Equation (37) can be presented as follows:

$$\begin{aligned} \dot{V}_4 &\leq -k_{5,v,i}e_{v,i}^2 - k_{4,v,i}\hat{d}_{v,i}^2 - \frac{1}{2}k_{2,v,i}\|\tilde{W}_{v,i}\|^2 + \frac{1}{2}\|e_{v,i}\|^2 + \frac{1}{2}\bar{d}_{v,i}^2 + k_{2,v,i}\frac{1}{2}\|\bar{W}_{v,i}\|^2 \\ &\leq -(k_{5,v,i} - \frac{1}{2})e_{v,i}^2 - k_{4,v,i}\hat{d}_{v,i}^2 - \frac{1}{2}k_{2,v,i}\|\tilde{W}_{v,i}\|^2 + \frac{1}{2}\bar{d}_{v,i}^2 + k_{2,v,i}\frac{1}{2}\|\bar{W}_{v,i}\|^2. \end{aligned} \tag{40}$$

Thus, it can be concluded that $\dot{V}_4 \leq -\sigma_4 V_4 + \zeta_2$ with

$$\sigma_4 = \min\left\{k_{5,v,i} - \frac{1}{2}, k_{4,v,i}, \frac{1}{2}k_{2,v,i}\right\} > 0 \tag{41}$$

and

$$\zeta_2 = \frac{1}{2}d_{v,i}^2 + k_{2,v,i} \frac{1}{2} \|\bar{W}_{v,i}\|^2 > 0. \tag{42}$$

3.4. Stability Analysis

Consider the Lyapunov candidate represented as follows:

$$\begin{aligned} V &= V_1 + V_2 + V_3 + V_4 \\ &= \frac{b_{x,i}^2}{\pi} \tan\left(\frac{\pi x_{e,i}^2}{2b_{x,i}^2}\right) + \frac{b_{y,i}^2}{\pi} \tan\left(\frac{\pi y_{e,i}^2}{2b_{y,i}^2}\right) \\ &\quad + \frac{1}{2}e_{\theta,i}^2 + \frac{1}{2}k_{3,\theta,i}^{-1}d_{\theta,i}^2 + \frac{1}{2}k_{1,\theta,i}^{-1}\bar{W}_{\theta,i}^2 + \frac{1}{2}e_{v,i}^2 + \frac{1}{2}k_{3,v,i}^{-1}d_{v,i}^2 + \frac{1}{2}k_{1,v,i}^{-1}\bar{W}_{v,i}^2. \end{aligned} \tag{43}$$

It concludes that $\dot{V} \leq -\sigma V + \zeta$, where

$$\sigma = \min\left\{k_d - 2k_b, k_v - 2k_c, k_{5,\theta,i} - \frac{1}{2}, k_{4,\theta,i}, k_{2,\theta,i}, k_{5,v,i} - \frac{1}{2}, k_{4,v,i}, k_{2,v,i}\right\} > 0 \tag{44}$$

and

$$\zeta = \frac{1}{2}d_{v,i}^2 + k_{2,v,i} \frac{1}{2} \|\bar{W}_{v,i}\|^2 + \frac{1}{2}d_{\theta,i}^2 + k_{2,\theta,i} \frac{1}{2} \|\bar{W}_{\theta,i}\|^2 > 0. \tag{45}$$

Choosing parameters such that $k_d > 2k_b$, $k_v > 2k_c$, $k_{5,\theta,i} > \frac{1}{2}$, and $k_{5,v,i} > \frac{1}{2}$, and integrating Equation (43), it can derive the inequality $V \leq \left(V(0) - \frac{\zeta}{\sigma}\right)e^{-\sigma t} + \frac{\zeta}{\sigma}$. There, it can be concluded that V is bounded. Moreover, $\frac{b_{x,i}^2}{\pi} \tan\left(\frac{\pi x_{e,i}^2}{2b_{x,i}^2}\right) \leq V \leq \left(V(0) - \frac{\zeta}{\sigma}\right)e^{-\sigma t} + \frac{\zeta}{\sigma}$ and $\frac{b_{y,i}^2}{\pi} \tan\left(\frac{\pi y_{e,i}^2}{2b_{y,i}^2}\right) \leq V \leq \left(V(0) - \frac{\zeta}{\sigma}\right)e^{-\sigma t} + \frac{\zeta}{\sigma}$ imply that the following constraints hold:

$$x_{e,i}^2 \leq \frac{2b_{x,i}^2}{\pi} \tan^{-1}\left(\frac{\pi}{b_{x,i}^2} \left(\left(V(0) - \frac{\zeta}{\sigma}\right)e^{-\sigma t} + \frac{\zeta}{\sigma}\right)\right) < b_{x,i}^2 \tag{46}$$

and

$$y_{e,i}^2 \leq \frac{2b_{y,i}^2}{\pi} \tan^{-1}\left(\frac{\pi}{b_{y,i}^2} \left(\left(V(0) - \frac{\zeta}{\sigma}\right)e^{-\sigma t} + \frac{\zeta}{\sigma}\right)\right) < b_{y,i}^2. \tag{47}$$

Hence, it can be concluded that $x_{e,i}$ and $y_{e,i}$ are constrained such that $|x_{e,i}| < |b_{x,i}|$ and $|y_{e,i}| < |b_{y,i}|$. Ultimately, these terms can be reduced to a narrow vicinity around zero.

4. Simulation Results

In this section, the simulation results are presented to demonstrate formation control under various disturbances. To highlight the performance of the proposed approach clearly, the controller is compared with the conventional controller, which does not employ the PPC method in the simulation results. Main parameters of the controller are listed in Table 1. Vehicle 1 serves as the leader, and Vehicles 2 to 6 act as the followers in the simulation. The leader’s desired trajectory, denoted as $(x_1(t), y_1(t))$, follows the equations $x_1(t) = 2 \sin(\frac{t}{10}) + 2 \cos(\frac{t}{5})$ and $y_1(t) = 2t$. The vehicles are arranged in a hexagonal formation, with each side measuring 10 m in length. Initially, Vehicles 2 to 6 are positioned

at $(2, -9.9)$, $(-6.5, -15)$, $(-6.5, 15)$, $(-15.5, 0.1)$, and $(-6.5, 5.1)$, respectively. The velocity of the leader is set as $v(t) = \sqrt{(\frac{2}{10} \cos(\frac{t}{10}) - \frac{2}{5} \sin(\frac{t}{5}))^2 + 2^2}$. The heading angle of the object is set as $\psi(t) = \text{atan2}(\frac{2}{10} \cos(\frac{t}{10}) - \frac{2}{5} \sin(\frac{t}{5}), 2)$.

When modeling dynamic systems subject to random perturbations $\chi(t)$, the stochastic differential equation as follows is utilized:

$$\dot{\chi}(t) = -2\chi(t) + u(t) - 0.5, \tag{48}$$

where $u(t)$ follows a standard normal distributed random process. This equation characterizes the evolution of external disturbances over time (refer to Figure 4).

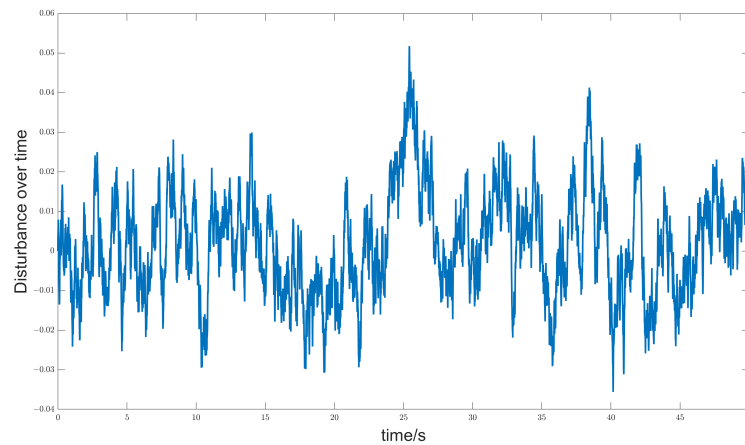


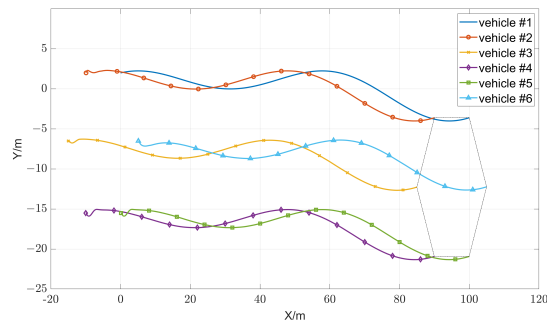
Figure 4. An example of external disturbance $\chi(t)$.

Table 1. Main parameters of the controller.

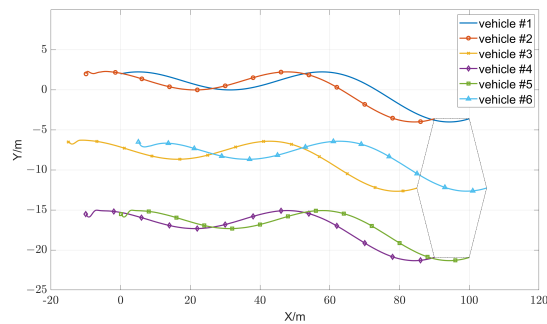
Parameter	Value	Parameter	Value
k_y	0.1	$k_{4,\theta,i}$	0.01
k_v	0.1	$k_{5,\theta,i}$	2
$k_{1,\theta,i}$	0.5	$k_{3,v,i}$	1
$k_{2,\theta,i}$	8	$k_{4,v,i}$	1
$k_{1,v,i}$	5	$k_{5,v,i}$	0.2
$k_{2,v,i}$	18	ζ_0	0.8
$k_{3,\theta,i}$	10	ω_{n0}	20

Figure 5 shows the vehicle formation trajectories under different controllers, comparing results with and without the proposed PPC method. From the shape of the trajectories, it is evident that both controllers effectively maintained the formation during movement and ensured a smooth motion trajectory. This demonstrates the efficacy of the designed guidance laws, neural networks, and adaptive laws. The simulation results presented in Figures 6 and 7 provide a comprehensive analysis of the effectiveness of the formation control algorithm in minimizing trajectory tracking errors for the followers. Furthermore, these results clearly demonstrate that controllers utilizing the PPC method are more effective at reducing tracking errors than those without the PPC method.

Initially, the position errors along the x and y axes for the followers are approximately 1 m, which can be attributed to random initial conditions. However, as the simulation progresses, the formation control algorithm effectively guides the followers towards their target positions, leading to a rapid convergence of position errors. Within a short period, the errors decreased significantly, demonstrating the high precision and effectiveness achieved by the control strategy. It is clear that the error curves for controllers without the PPC method converge more slowly and exhibit higher maximum error values compared to those with the PPC method.



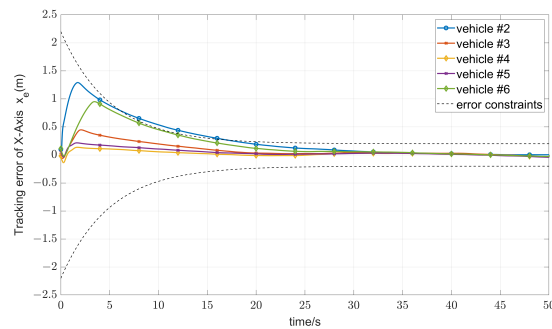
(a)



(b)

Figure 5. Trajectory of formation with different cases: (a) Without PPC method and (b) with PPC method.

The figures also showcase the error constraints, which define the acceptable range of position errors during operation (0.25 m). As shown in Figures 6 and 7, the control errors with the PPC method are confined within the preset constraints throughout the entire simulation process, whereas the errors without the PPC method exceed the constraints before converging and ultimately settle at a noticeably higher level compared to those with the PPC method.



(a)

Figure 6. Cont.

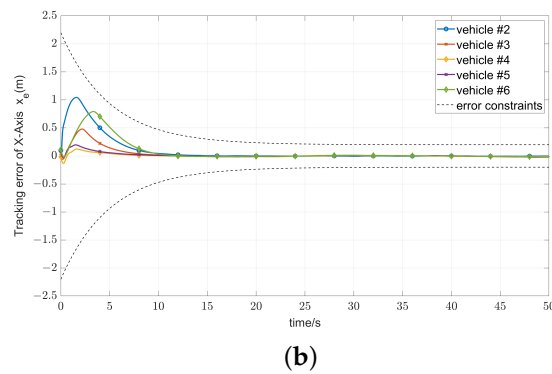


Figure 6. Trajectory tracking error of x-axis with different methods: (a) without PPC method and (b) with PPC method.

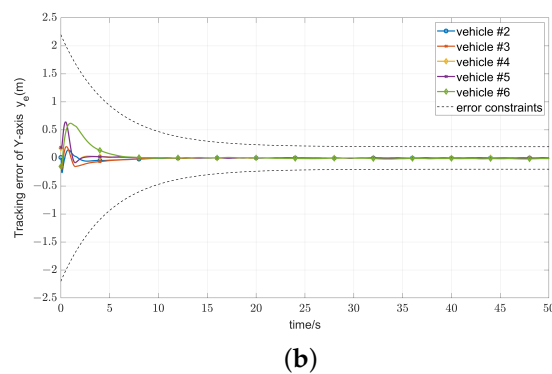
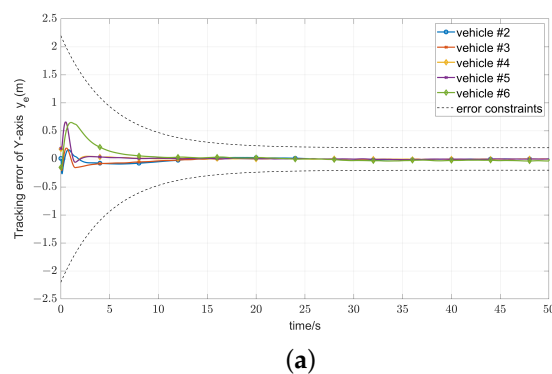
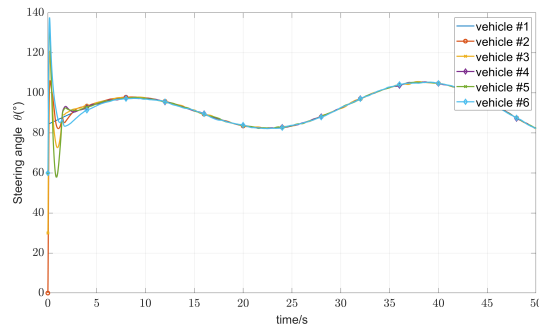


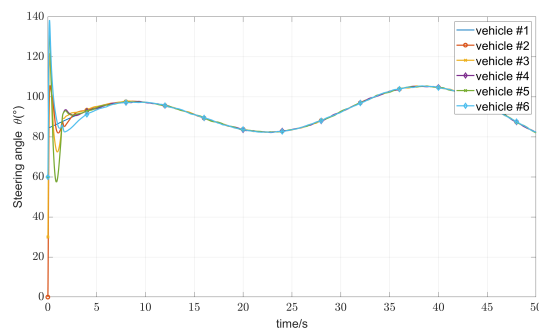
Figure 7. Trajectory tracking error of y-axis with different methods: (a) Without PPC and (b) with PPC.

As depicted in Figure 8, the leader’s angular change exhibits a smooth transition. In the initial startup phase (approximately the first 2 s), the five followers swiftly adjust their angles within a range of 58 to 140 degrees. Subsequently, they converge to a narrower variation range of 90 to 100 degrees. Based on the overlap of the curve colors, the convergence speed of the error for controllers with the PPC method is slightly higher than that of controllers without the PPC method.

The velocity progression of the formation members is illustrated in Figure 9. Within the initial three seconds, all followers rapidly converge their speeds to a range of 1.8–2.5 m/s and subsequently maintain a speed almost consistent with that of Vehicle 1. It is noteworthy that the speed of controllers with the PPC method converges well around 12 s, whereas the speed outputs of controllers without the PPC method only converge well after 15 s. This further demonstrates that controllers incorporating the PPC method are more stable.



(a)

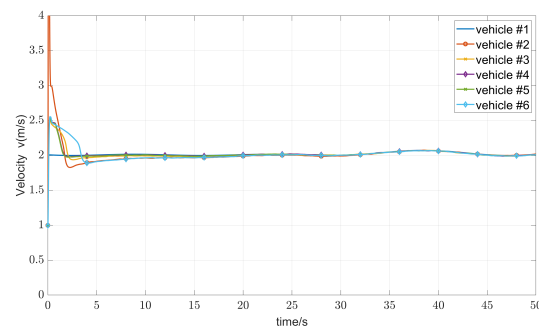


(b)

Figure 8. Steering angle error of formation with different methods: (a) Without PPC and (b) with PPC.

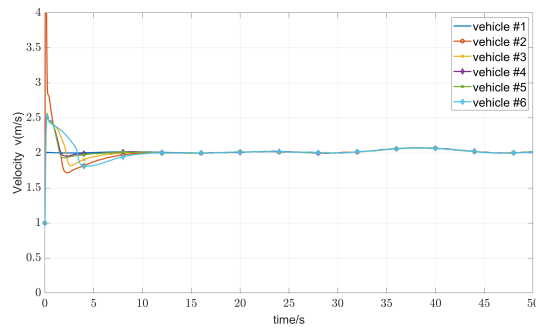
Figures 10–14 depict the control inputs applied to the followers under various disturbances. The inputs rapidly converge, demonstrating the stability of the approach.

To provide a more detailed depiction of the results, the Mean Squared Error and maximum error of the position will be shown to more clearly reflect its performance. For the i -th follower, the mean squared position error u_i is calculated as $u_i = \frac{1}{N} \sum_{t=1}^N (e_i(t))^2$, where $e_i(t) = \sqrt{x_{e,i}^2(t) + y_{e,i}^2(t)}$ represents the position error at time step t , and N is the total number of samples. The maximal position error for the i -th follower m_i can be calculated as $m_i = \max_{t=1}^N \{e_i(t)\}$.



(a)

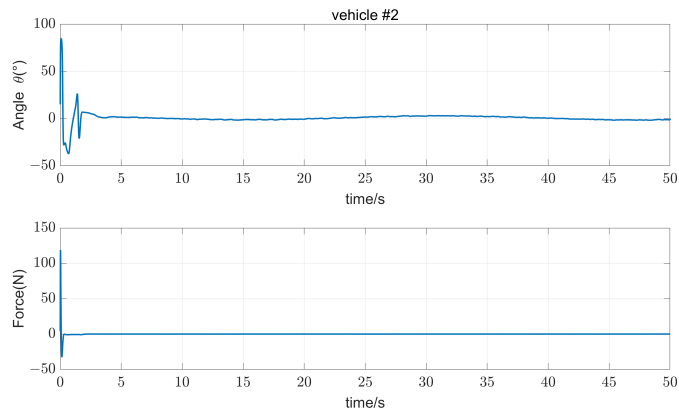
Figure 9. Cont.



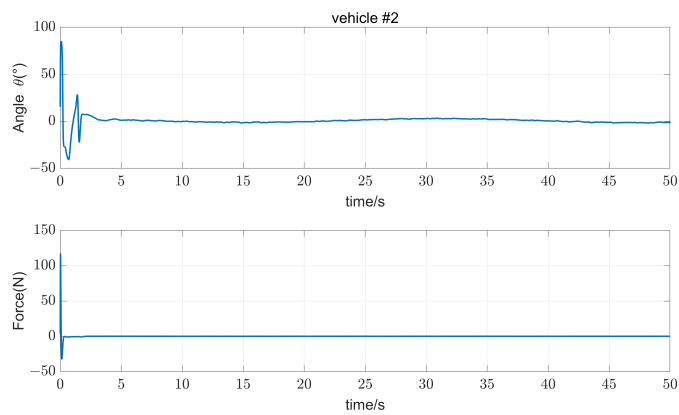
(b)

Figure 9. Vehicle velocity with different methods: (a) Without PPC and (b) with PPC.

The results, as shown in Table 2, clearly demonstrate the superior performance of the proposed controller compared to the conventional one (without PPC), which aligns with expectations.



(a)



(b)

Figure 10. Control inputs of Vehicle 2 with different methods: (a) Without PPC (b) with PPC.

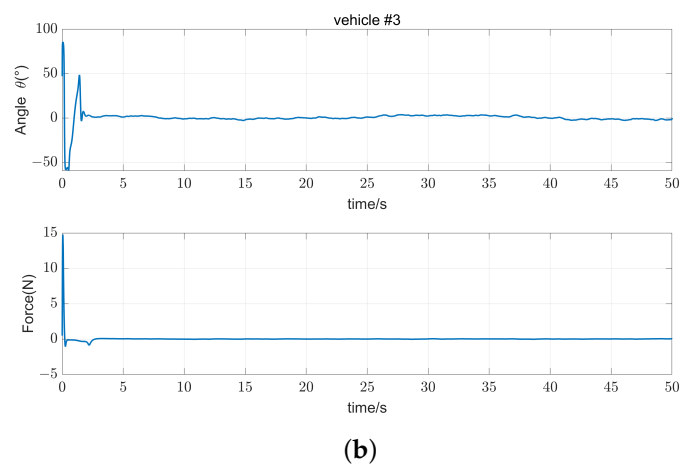
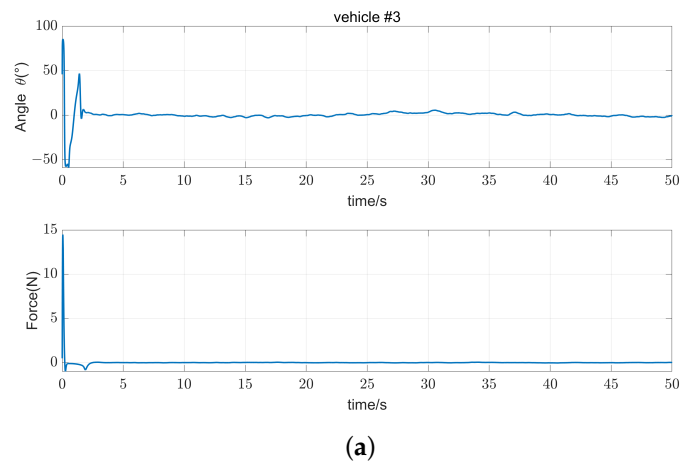


Figure 11. Control inputs of Vehicle 3 with different methods: (a) Without PPC and (b) with PPC.

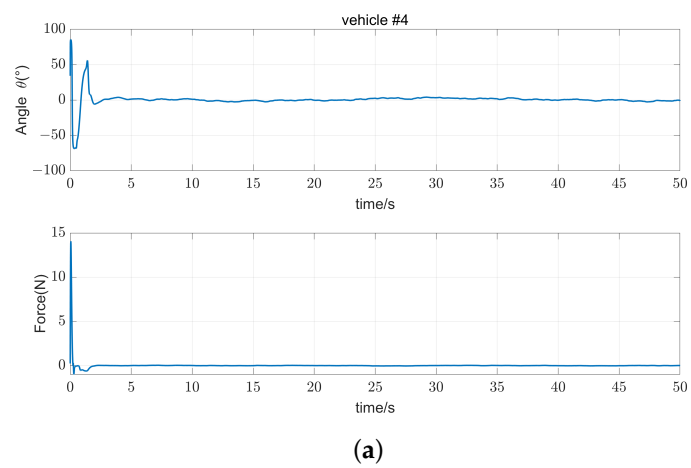


Figure 12. Cont.

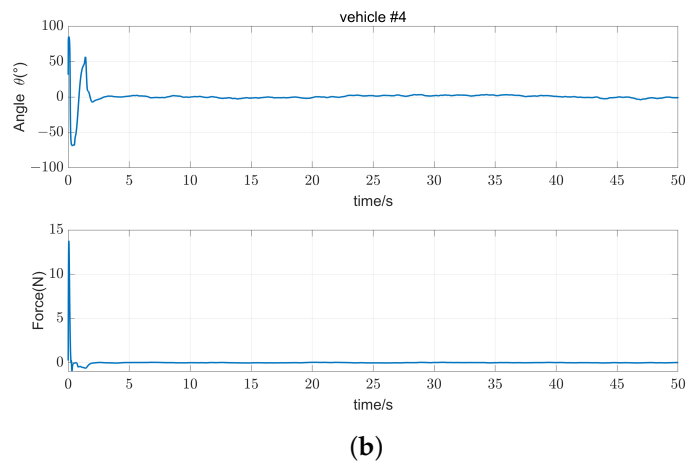


Figure 12. Control inputs of Vehicle 4 with different methods: (a) Without PPC and (b) with PPC.

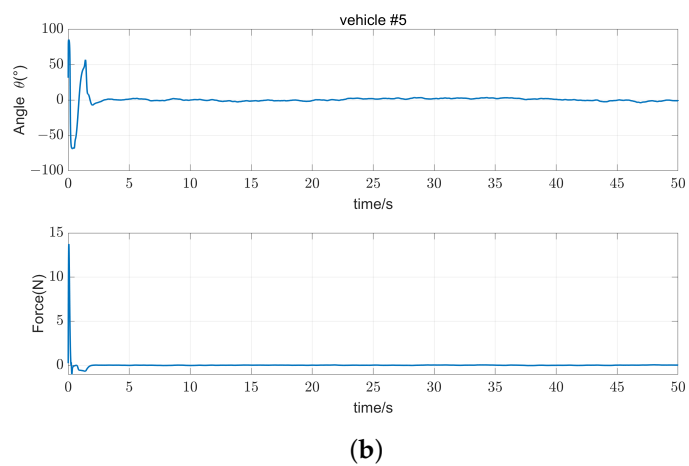
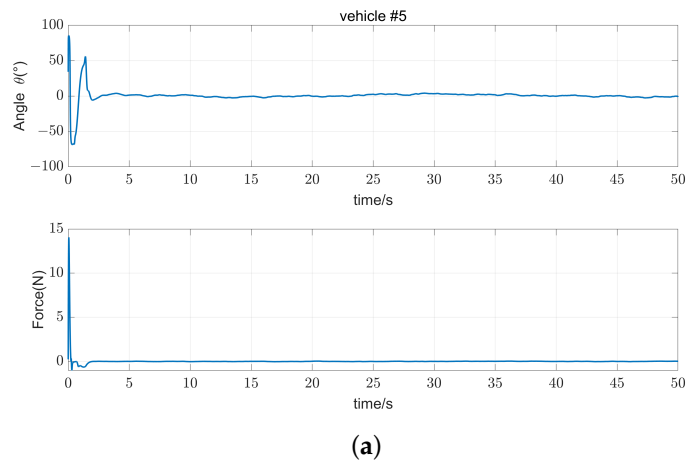


Figure 13. Control inputs of Vehicle 5 with different methods: (a) Without PPC and (b) with PPC.

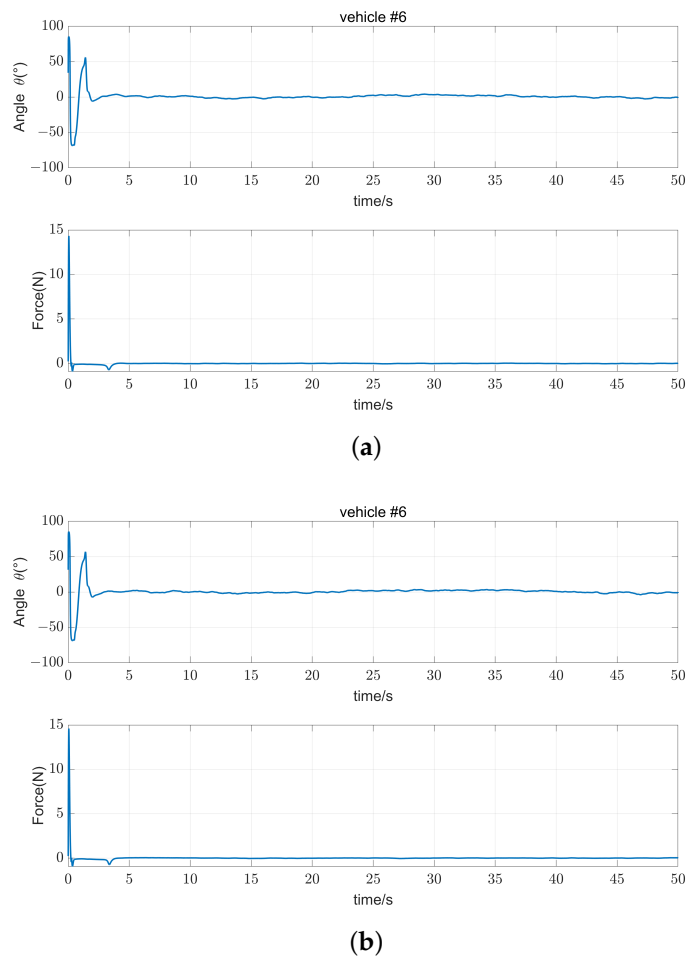


Figure 14. Control inputs of Vehicle 6 with different methods: (a) Without PPC and (b) with PPC.

Table 2. The mean square (u) and maximal (m) position errors of vehicles in meters.

Vehicle	u (Without PPC)	u (With PPC)	m (Without PPC)	m (With PPC)
2	0.1870	0.0570	1.2975	1.0334
3	0.0242	0.0114	0.4422	0.5004
4	0.0073	0.0051	0.6607	0.6452
5	0.0111	0.0060	0.6646	0.6470
6	0.1360	0.0604	0.9094	0.8705

5. Conclusions

This paper introduces an adaptive leader–follower formation controller with prescribed performance. The guidance law computes the desired velocity and steering angle based on the leader’s trajectory and a predefined formation pattern. To address challenges posed by unknown functions and external disturbances, a second-order filter and an RBFNN, alongside an adaptive law, are employed. Notably, the entire controller adheres to a backstepping method, incorporating distinct velocity and corner controllers to enhance system robustness. Furthermore, the inclusion of a barrier in the Lyapunov function contributes to achieving the prescribed performance. Simulation results illustrate that the proposed controller consistently attains superior performance within the specified limits, even in the presence of various disturbances.

Author Contributions: Conceptualization, F.X. and G.L.; methodology, F.X.; software, F.X.; validation, Y.-R.C., F.X. and G.L.; formal analysis, Y.-R.C., F.X. and G.L.; investigation, F.X.; resources, Y.-R.C. and F.X.; data curation, F.X. and G.L.; supervision, Y.-R.C.; writing—original draft preparation, Y.-R.C., F.X. and G.L.; writing—review and editing, Y.-R.C. and F.X.; project administration, Y.-R.C.; funding acquisition, Y.-R.C. All authors have read and agreed to the published version of the manuscript.

Funding: This work was supported in part by the National Science and Technology Council, Taiwan (NSTC) under Grant 112-2221-E-197-022.

Data Availability Statement: The article includes all the data supporting the results, and there was no need for any extra source data.

Acknowledgments: The authors would like to thank all the reviewers for their constructive comments.

Conflicts of Interest: The authors declare no conflicts of interest.

References

- Balch, T.; Arkin, R. Behavior-based formation control for multirobot teams. *IEEE Trans. Robot. Autom.* **1998**, *14*, 926–939. [[CrossRef](#)]
- Do, K. Formation control of multiple elliptical agents with limited sensing ranges. *Automatica* **2012**, *48*, 1330–1338. [[CrossRef](#)]
- Li, X.; Pei, G.; Liu, L.; Chen, L.; Zhang, W. Metabolomic analysis and lipid accumulation in a glucose tolerant *Cryptocodium* strain obtained by adaptive laboratory evolution. *Bioresour. Technol.* **2017**, *235*, 87–95. [[CrossRef](#)]
- Cao, Y.; Yu, W.; Ren, W.; Chen, G. An Overview of Recent Progress in the Study of Distributed Multi-Agent Coordination. *IEEE Trans. Ind. Inform.* **2013**, *9*, 427–438. [[CrossRef](#)]
- Yuan, C.; He, H.; Wang, C. Cooperative Deterministic Learning-Based Formation Control for a Group of Nonlinear Uncertain Mechanical Systems. *IEEE Trans. Ind. Inform.* **2019**, *15*, 319–333. [[CrossRef](#)]
- He, S.; Wang, M.; Dai, S.L.; Luo, F. Leader–Follower Formation Control of USVs With Prescribed Performance and Collision Avoidance. *IEEE Trans. Ind. Inform.* **2019**, *15*, 572–581. [[CrossRef](#)]
- Yang, E.; Gu, D. Nonlinear Formation-Keeping and Mooring Control of Multiple Autonomous Underwater Vehicles. *IEEE/ASME Trans. Mechatron.* **2007**, *12*, 164–178. [[CrossRef](#)]
- Breivik, M.; Hovstein, V.E.; Fossen, T.I. Ship Formation Control: A Guided Leader-Follower Approach. *IFAC Proc. Vol.* **2008**, *41*, 16008–16014. [[CrossRef](#)]
- Zhang, L.; Tao, R.; Zhang, Z.X.; Chien, Y.R.; Bai, J. PMSM non-singular fast terminal sliding mode control with disturbance compensation. *Inf. Sci.* **2023**, *642*, 119040. [[CrossRef](#)]
- Wu, H.M.; Karkoub, M.; Hwang, C.L. Mixed Fuzzy Sliding-Mode Tracking with Backstepping Formation Control for Multi-Nonholonomic Mobile Robots Subject to Uncertainties. *J. Intell. Robot. Syst.* **2015**, *79*, 73–86. [[CrossRef](#)]
- Wang, J.; Wang, C.; Wei, Y.; Zhang, C. Neuroadaptive Sliding Mode Formation Control of Autonomous Underwater Vehicles With Uncertain Dynamics. *IEEE Syst. J.* **2020**, *14*, 3325–3333. [[CrossRef](#)]
- Zhang, L.; Bai, J.; Wu, J. Speed Sensor-Less Control System of Surface-Mounted Permanent Magnet Synchronous Motor Based on Adaptive Feedback Gain Supertwisting Sliding Mode Observer. *J. Sens.* **2021**, *2021*, 8301359. [[CrossRef](#)]
- Su, B.; bin Wang, H.; Wang, Y. Dynamic event-triggered formation control for AUVs with fixed-time integral sliding mode disturbance observer. *Ocean Eng.* **2021**, *240*, 109893. [[CrossRef](#)]
- Zhang, L.; Wang, S.; Bai, J. Fast-super-twisting sliding mode speed loop control of permanent magnet synchronous motor based on SVM-DTC. *IEICE Electron. Express* **2020**, *18*, 20200375. [[CrossRef](#)]
- Rout, R.; Subudhi, B. A backstepping approach for the formation control of multiple autonomous underwater vehicles using a leader–follower strategy. *J. Mar. Eng. Technol.* **2016**, *15*, 38–46. [[CrossRef](#)]
- Pang, S.; Wang, J.; Liu, J.; Yi, H. Three-dimensional leader–follower formation control of multiple autonomous underwater vehicles based on line-of-sight measurements using the backstepping method. *Proc. Inst. Mech. Eng. Part I J. Syst. Control Eng.* **2018**, *232*, 819–829. [[CrossRef](#)]
- Mu, C.; Wei, X.; Zhang, H.; Hu, X.; Han, J. Disturbance observer-based backstepping control for leader–follower ships with disturbances. *Ships Offshore Struct.* **2023**, *19*, 532–540. [[CrossRef](#)]
- Wang, F.; Gao, Y.; Zhou, C.; Zong, Q. Disturbance observer-based backstepping formation control of multiple quadrotors with asymmetric output error constraints. *Appl. Math. Comput.* **2022**, *415*, 126693. [[CrossRef](#)]
- Zaidi, A.; Kazim, M.; Wang, H. A Robust Backstepping Sliding Mode Controller with Chattering-Free Strategy for a Swarm of Drones. *J. Phys. Conf. Ser.* **2022**, *2213*, 012007. [[CrossRef](#)]
- Yang, K.; Dong, W.; Tong, Y.; He, L. Leader-follower Formation Consensus of Quadrotor UAVs Based on Prescribed Performance Adaptive Constrained Backstepping Control. *Int. J. Control Autom. Syst.* **2022**, *20*, 3138–3154. [[CrossRef](#)]
- Oubelaid, A.; Taib, N.; Rekioua, T. Novel coordinated power sources switching strategy for transient performance enhancement of hybrid electric vehicles. *COMPEL Int. J. Comput. Math. Electr. Electron. Eng.* **2022**, *41*, 1880–1919. [[CrossRef](#)]
- Oubelaid, A.; Taib, N.; Nikolovski, S.; Alharbi, T.E.; Rekioua, T.; Flah, A.; Ghoneim, S.S. Intelligent speed control and performance investigation of a vector controlled electric vehicle considering driving cycles. *Electronics* **2022**, *11*, 1925. [[CrossRef](#)]

23. Oubelaid, A.; Albalawi, F.; Rekioua, T.; Ghoneim, S.S.; Taib, N.; Abdelwahab, S.A.M. Intelligent torque allocation based coordinated switching strategy for comfort enhancement of hybrid electric vehicles. *IEEE Access* **2022**, *10*, 58097–58115. [[CrossRef](#)]
24. Shojaei, K. Neural adaptive PID formation control of car-like mobile robots without velocity measurements. *Adv. Robot.* **2017**, *31*, 947–964. [[CrossRef](#)]
25. Jia, Z.; Wang, L.; Yu, J.; Ai, X. Distributed adaptive neural networks leader-following formation control for quadrotors with directed switching topologies. *ISA Trans.* **2019**, *93*, 93–107. [[CrossRef](#)]
26. Kuo, C.W.; Tsai, C.C.; Lee, C.T. Intelligent Leader-Following Consensus Formation Control Using Recurrent Neural Networks for Small-Size Unmanned Helicopters. *IEEE Trans. Syst. Man Cybern. Syst.* **2021**, *51*, 1288–1301. [[CrossRef](#)]
27. Huang, C.; Zhang, X.; Zhang, G. Adaptive neural finite-time formation control for multiple underactuated vessels with actuator faults. *Ocean Eng.* **2021**, *222*, 108556. [[CrossRef](#)]
28. Rani, M.; Kumar, N. A neural network based efficient leader–follower formation control approach for multiple autonomous underwater vehicles. *Eng. Appl. Artif. Intell.* **2023**, *122*, 106102. [[CrossRef](#)]
29. Zhao, X.; Chen, S.; Zhang, Z.; Zheng, Y. Consensus Tracking for High-Order Uncertain Nonlinear MASs via Adaptive Backstepping Approach. *IEEE Trans. Cybern.* **2023**, *53*, 1248–1259. [[CrossRef](#)]
30. Huang, H.; Gong, M.; Zhuang, Y.; Sharma, S.; Xu, D. A new guidance law for trajectory tracking of an underactuated unmanned surface vehicle with parameter perturbations. *Ocean Eng.* **2019**, *175*, 217–222. [[CrossRef](#)]
31. Xia, Y.; Xu, K.; Li, Y.; Xu, G.; Xiang, X. Improved line-of-sight trajectory tracking control of under-actuated AUV subjects to ocean currents and input saturation. *Ocean Eng.* **2019**, *174*, 14–30. [[CrossRef](#)]
32. Rout, R.; Cui, R.; Han, Z. Modified Line-of-Sight Guidance Law With Adaptive Neural Network Control of Underactuated Marine Vehicles With State and Input Constraints. *IEEE Trans. Control Syst. Technol.* **2020**, *28*, 1902–1914. [[CrossRef](#)]
33. Bechlioulis, C.P.; Rovithakis, G.A. Robust Adaptive Control of Feedback Linearizable MIMO Nonlinear Systems With Prescribed Performance. *IEEE Trans. Autom. Control* **2008**, *53*, 2090–2099. [[CrossRef](#)]
34. Wang, M.; Yang, A. Dynamic Learning From Adaptive Neural Control of Robot Manipulators With Prescribed Performance. *IEEE Trans. Syst. Man Cybern. Syst.* **2017**, *47*, 2244–2255. [[CrossRef](#)]
35. Dai, S.L.; He, S.; Chen, X.; Jin, X. Adaptive Leader–Follower Formation Control of Nonholonomic Mobile Robots With Prescribed Transient and Steady-State Performance. *IEEE Trans. Ind. Inform.* **2020**, *16*, 3662–3671. [[CrossRef](#)]
36. Jiang, Y.; Liu, Z.; Chen, Z. Prescribed-time distributed formation control for a class of nonlinear multi-agent systems subject to internal uncertainties and external disturbances. *Nonlinear Dyn.* **2023**, *111*, 1643–1655. [[CrossRef](#)]
37. Dai, S.L.; He, S.; Cai, H.; Yang, C. Adaptive Leader–Follower Formation Control of Underactuated Surface Vehicles with Guaranteed Performance. *IEEE Trans. Syst. Man Cybern. Syst.* **2022**, *52*, 1997–2008. [[CrossRef](#)]
38. Mehdifar, F.; Bechlioulis, C.P.; Hashemzadeh, F.; Baradarannia, M. Prescribed performance distance-based formation control of Multi-Agent Systems. *Automatica* **2020**, *119*, 109086. [[CrossRef](#)]
39. Verginis, C.K.; Bechlioulis, C.P.; Dimarogonas, D.V.; Kyriakopoulos, K.J. Robust Distributed Control Protocols for Large Vehicular Platoons With Prescribed Transient and Steady-State Performance. *IEEE Trans. Control Syst. Technol.* **2018**, *26*, 299–304. [[CrossRef](#)]
40. Fan, B.; Yang, Q.; Jagannathan, S.; Sun, Y. Output-Constrained Control of Nonaffine Multiagent Systems With Partially Unknown Control Directions. *IEEE Trans. Autom. Control* **2019**, *64*, 3936–3942. [[CrossRef](#)]

Disclaimer/Publisher’s Note: The statements, opinions and data contained in all publications are solely those of the individual author(s) and contributor(s) and not of MDPI and/or the editor(s). MDPI and/or the editor(s) disclaim responsibility for any injury to people or property resulting from any ideas, methods, instructions or products referred to in the content.